DESIGN OF DETACHED BREAKWATERS FOR COASTAL PROTECTION: DEVELOPMENT AND APPLICATION OF AN ADVANCED NUMERICAL MODEL

Theophanis V. Karambas[1]

An advanced nonlinear wave, sediment transport and bed morphology evolution 2DH model, for the design of coastal protection structures, has been developed. The extended Boussinesq equations, including higher order non-linear terms, which can describe the propagation of highly nonlinear waves in the shoaling region, surf and swash zone, are used. The bed and suspended load transport are estimated with a quasi-steady, semi-empirical formulation, developed by Camenen, and Larson ('A unified sediment transport formulation for coastal inlet application', *Technical report ERDC/CHL CR-07-1*, US Army Engineer Research and Development Center, Vicksburg, MS, 2007) for an oscillatory flow combined with a superimposed current under an arbitrary angle, involving phase-lag effects in the sheet flow layer. Model results are compared with experimental data (morphology evolution behind detached breakwaters). The agreement between numerical simulations and data is quite satisfactory. Also, model predictions agree with the tombolo/salient criteria found in the literature. The methodology can be applied to the design of detached breakwaters, which are used as coastal protection structures.

Keywords: detached breakwaters, coastal protection structures numerical modeling, Boussinesq model, sediment transport

INRODUCTION

A proper design of the coastal protection structures, such as detached emerged and submerged breakwaters, requires the use of advanced mathematical models, able to simulate the complicated hydro-morphodynamic processes of the nearshore region (including swash zone), such as nonlinear wave propagation, wave-induced current, sediment transport by waves and currents and bed morphology evolution. The Boussinesq models and their combination with a sediment transport model seem to be suitable for the above purpose (Rakha et al., 1997, Karambas and Koutitas, 2002, Karambas, 2002 & 2004, Karambas and Karathanassi, 2004). These models have the advantage that they can incorporate nonlinear breaking and non breaking irregular wave propagation from deep to shallow water and the swash zone. The models include the prediction of quasi-3D currents and long waves and provide to the sediment transport formulae all the required information such as, breaking wave induced turbulence, near bed velocity asymmetry and acceleration, swash zone modeling etc. (Rakha et al., 1997, Karambas and Koutitas, 2002, Karambas, 2002 & 2004, Wenneker et al., 2011).

In the present work, the non linear wave transformation in the surf and swash zone is computed by a non-linear breaking wave model based on the higher order Boussinesq equations for breaking and non breaking waves. The Camenen and Larson (2005, 2007, 2008) transport rate formula involving unsteady aspects of the sand transport phenomenon is adopted for estimating bed load as well as and suspended load. The model is applied to simulate sediment transport and beach evolution behind detached breakwaters used for coastal protection.

WAVE AND CURRENT MODULE

The Boussinesq equations have been shown to be capable of reproducing successfully the wave phenomena that affect the morphology of the coastal area. The classical Boussinesq equations have been extended so as to be able to include higher order non-linear terms, which can describe better the propagation of highly nonlinear waves in the shoaling zone. Apart from that, the linear dispersion characteristics of the equations have been improved in order to describe the nonlinear wave propagation from deeper waters (Zou, 1999).

Wave energy dissipation due to wave breaking is usually based on a significant characteristic of a breaker: the presence of the surface roller. Dissipation due to the roller can be introduced as an excess momentum term due to the non-uniform velocity distribution (Schäffer et al., 1993). Schäffer et al. (1993) are based on a simplified velocity profile where the surface roller is being transported with the wave celerity $\boldsymbol{c}=(c_x,c_y)$:

[1] School of Civil Engineering, Dept. of Hydraulics and Environmental Engineering, Aristotle University of Thessaloniki, 54624, Thessaloniki, Greece

$$\begin{aligned} &u=c_x \ , v=c_y \quad \text{for} \quad \zeta-\delta \le z \le \zeta \\ &u=u_o \ , \ v=v_o \quad \text{for} \quad -d \le z \le \zeta-\delta \end{aligned} \tag{1}$$

where (c_x,c_y)=wave celerities in the x- (cross-shore) and y- directions (alongshore); and (u_o,v_o)=bottom velocities in the x-and y- directions.

Based on the previous velocity profile, the following higher order Boussinesq-type equations for breaking and nonbreaking waves can be derived (Zou 1999; Karambas and Koutitas 2002, Karambas and Karathanassi, 2004):

$$\zeta_t + \nabla(h\mathbf{U}) = 0$$

$$\mathbf{U}_t + \frac{1}{h}\nabla\mathbf{M}_u - \frac{1}{h}\mathbf{U}\nabla(\mathbf{U}h) + g\nabla\zeta + G = \frac{1}{2}h\nabla\left[\nabla\cdot(d\mathbf{U}_t)\right] - \frac{1}{6}h^2\nabla\left[\nabla\cdot\mathbf{U}_t\right] + \frac{1}{30}d^2\nabla\left[\nabla\cdot(\mathbf{U}_t + g\nabla\zeta)\right] + \frac{1}{30}\nabla\left[\nabla\cdot\left(d^2\mathbf{U}_t + gd^2\nabla\zeta\right)\right] - d\nabla(\delta\nabla\cdot\mathbf{U})_t - \frac{\boldsymbol{\tau}_b}{h} + \mathbf{E} \tag{2}$$

where

$$G = \frac{1}{3}\nabla\left\{d^2\left[(\nabla\cdot\mathbf{U})^2 - \mathbf{U}\cdot\nabla^2\mathbf{U} - \frac{1}{10}\nabla^2(\mathbf{U}\cdot\mathbf{U})\right]\right\} - \frac{1}{2}\zeta\nabla\left[\nabla\cdot(d\mathbf{U}_t)\right]$$

where subscript t denotes differentiation with respect to time; d=still water depth; U=horizontal velocity vector, $\mathbf{U}=(U,V)$, where U and V=depth-averaged horizontal velocities in directions x and y; ζ=surface elevation, h=total depth $h=d+\zeta$, g=gravitational acceleration, $\boldsymbol{\tau}_b=(\tau_{bx},\ \tau_{by})$= bottom friction term; δ=roller thickness (determined geometrically according to Schäffer et al. 1993), **E**=eddy viscosity term (according to Chen et al. 1999); and $\mathbf{M}_u=(d+\zeta)\ \mathbf{u_o}^2+\delta(c^2-\mathbf{u_o}^2)$, in which $\mathbf{u_o}=(u_o\ ,v_o)$. The roller celerity $\mathbf{c}=(c_x,c_y)$ is computed by using (Sørensen et al., 1998):

$$c_x = \frac{\partial\zeta}{\partial x}\frac{1.3\sqrt{gd}}{\sqrt{\left(\frac{\partial\zeta}{\partial x}\right)^2+\left(\frac{\partial\zeta}{\partial y}\right)^2}} \qquad c_y = \frac{\partial\zeta}{\partial y}\frac{1.3\sqrt{gd}}{\sqrt{\left(\frac{\partial\zeta}{\partial x}\right)^2+\left(\frac{\partial\zeta}{\partial y}\right)^2}}$$

The above breaking procedure (i.e. surface roller concept) is valid only inside the inner region of the surf zone, where unsteady bores are formed and propagate over a sloping bottom. In the swash zone the bore collapses at the shore, surface rollers are not present and consequently the velocity distribution given by Eq. (1) is not valid. Thus, this dissipation mechanism (i.e. surface roller concept) can not be applied in this region. Instead of this, the eddy viscosity concept is adopted in order to simulate the dissipation due to turbulence in the swash zone. The swash zone eddy viscosity coefficient ν_s is estimated from:

$$\nu_s = \ell_s\left[\left(\frac{\partial U}{\partial x}\right)^2+\left(\frac{\partial V}{\partial y}\right)^2+\frac{1}{2}\left(\frac{\partial U}{\partial y}+\frac{\partial V}{\partial x}\right)^2\right]^{1/2} \tag{3}$$

where ℓ_s is a length scale which is related to the total water depth h through $\ell_s=2h$ (Karambas and Koutitas, 2002).

In the swash zone, the 'dry bed' boundary condition is used to simulate runup. The condition, at a grid point *(i,j)*, is written (Militello et al., 2004):

if $(d+\zeta)_{i,j} > h_{cr}$ and $(d+\zeta)_{i-1,j} \le h_{cr}$ and $U_{i,j} > 0$ then $U_{i,j} = 0$
if $(d+\zeta)_{i,j} > h_{cr}$ and $(d+\zeta)_{i,j-1} \le h_{cr}$ and $V_{i,j} > 0$ then $V_{i,j} = 0$

if $(d+\zeta)_{i,j} \le h_{cr}$ and $(d+\zeta)_{i-1,j} \le h_{cr}$ then $U_{i,j} = 0$
if $(d+\zeta)_{i,j} \le h_{cr}$ and $(d+\zeta)_{i,j-1} \le h_{cr}$ then $V_{i,j} = 0$

if $(d+\zeta)_{i,j} \le h_{cr}$ and $(d+\zeta)_{i-1,j} > h_{cr}$ and $U_{i,j} < 0$ then $U_{i,j} = 0$
if $(d+\zeta)_{i,j} \le h_{cr}$ and $(d+\zeta)_{i,j-1} > h_{cr}$ and $V_{i,j} < 0$ then $V_{i,j} = 0$

where h_{cr} is a very small depth below which drying is assumed to occur. Here we consider h_{cr}=0.00001 m.

The above condition is very simple and very easily incorporated in a nonlinear wave model.

The bottom shear stresses term are approximated by the use of the formulae proposed by Kobayashi et al. (2007):

$$\tau_{bx} = \frac{1}{2}\rho f_b \sigma_T^2 G_{bx} \qquad \tau_{by} = \frac{1}{2}\rho f_b \sigma_T^2 G_{by} \tag{4}$$

with σ_T is the standard deviation of the oscillatory horizontal velocity, f_b is the bottom friction factor, and

$$G_{bx} = \frac{U_c}{\sigma_T}\left[1.16^2 + \left(\frac{U_c}{\sigma_T}\right)^2\right]^{-0.5} \qquad G_{by} = \frac{V_c}{\sigma_T}\left[1.16^2 + \left(\frac{V_c}{\sigma_T}\right)^2\right]^{-0.5}$$

where U_c and V_c are the depth averaged current velocities, estimated after time-averaging the instantaneous velocities U and V (according to Karambas and Karathanassi, 2004).

The governing equations are finite-differenced utilizing a high-order predictor-corrector scheme that employs a third-order explicit Adams-Bashforth predictor step and a fourth-order implicit Adams-Moulton corrector step (Wei and Kirby, 1995). The corrector step is iterated until the desirable convergence is achieved. First order spatial derivatives are discretized to fourth-order accuracy.

SEDIMENT TRANSPORT MODULE

The mode of sediment movement on the coast is usually divided into bed load, suspended load and sheet flow transport. Different model concepts are being presently used for the prediction of each one, which range from empirical transport formulas to more sophisticated bottom boundary layer models. In the present work, the bed load transport (q_{sb}) is estimated with a quasi-steady, semi-empirical formulation, developed by Camenen, and Larson, (2005, 2007, 2008) for an oscillatory flow combined with a superimposed current under an arbitrary angle:

$$\Phi_b = \begin{cases} \dfrac{q_{sb,w}}{\sqrt{(s-1)gd_{50}^{\,3}}} = a_n \sqrt{\theta_{cw,net}}\,\theta_{cw,m} \exp\left(-b\dfrac{\theta_{cr}}{\theta_{cw}}\right) \\ \dfrac{q_{sb,n}}{\sqrt{(s-1)gd_{50}^{\,3}}} = a_n \sqrt{\theta_{cn}}\,\theta_{cw,m} \exp\left(-b\dfrac{\theta_{cr}}{\theta_{cw}}\right) \end{cases} \tag{5}$$

where the subscripts *w* and *n* correspond, respectively, to the wave direction and the direction normal to the wave direction, *s* (= ρ_s/ρ) is the relative density between sediment (ρ_s) and water (ρ), *g* the acceleration due to gravity, d_{50} the median grain size, a_w, a_n and *b* are empirical coefficients (Camenen and Larson 2007), $\theta_{cw,m}$ and θ_{cw} the mean and maximum Shields parameters due to wave-current interaction, θ_{cn} the current-related Shields parameter in the direction normal to the wave direction, and θ_{cr} the critical Shields parameter for the inception of transport. The net Shields parameter $\theta_{cw,net}$ in eq. 5 is given by:

$$\theta_{cw,net} = \left(1 - a_{pl,b}\right)\theta_{cw,on} - \left(1 + a_{pl,b}\right)\theta_{cw,off} \tag{6}$$

where $\theta_{cw,on}$ and $\theta_{cw,off}$ are the mean values of the instantaneous Shields parameter over the two half periods T_{wc} and T_{wt} ($T_w = T_{wc} + T_{wt}$, in which T_w is the wave period and $\alpha_{pl,b}$ a coefficient for the phase-lag effects (Camenen and Larson 2007). The Shields parameter is defined by $\theta_{cw,j} = \frac{1}{2} f_{cw} U_{cw,j}^2 / \left[(s-1) g d_{50}\right]$, with U_{cw} being the wave and current velocity, f_{cw} the friction coefficient taking into account wave and current interaction and the subscript j should be replaced either by *onshore* or *offshore*.

Phase-lag effects in the sheet flow layer were included through the coefficient (Camenen and Larson, 2007):

$$a_{pl} = a_{onshore} - a_{offshore} \tag{7}$$

with

$$a_j = \frac{v^{0.25} U_{wj}^{0.5}}{w_s T_j^{0.75}} \exp\left[-\left(\frac{U_{w,crsf}}{U_{wj}} \right)^2 \right]$$

where *v* is the kinematic viscosity of water, $U_{w\,crsf}$, the critical velocity for the inception of sheet flow, U_w is the wave orbital velocity amplitude, W_s the sediment fall speed and the subscript j should be replaced either by *onshore* or *offshore*.

The suspended sediment load ($\boldsymbol{q_{ss}}$) may be obtained from (Camenen and Larson 2007):

$$\begin{aligned} q_{ss,x} &= U_c \frac{c_R \varepsilon}{W_s} \left[1 - \exp\left(-\frac{w_s h}{\varepsilon} \right) \right] \\ q_{ss,y} &= V_c \frac{c_R \varepsilon}{W_s} \left[1 - \exp\left(-\frac{w_s h}{\varepsilon} \right) \right] \end{aligned} \tag{8}$$

where c_R is the reference concentration at the bottom, ε the sediment diffusivity.

The bed reference concentration is written as follows based on the analysis of a large data set on sediment concentration profiles (Camenen and Larson, 2007):

$$c_R = 3.51^{-3} \exp\left(-0.3 d_*\right) \theta_{cw,m} \exp\left(-4.5 \frac{\theta_{cr}}{\theta_{cw}} \right) \tag{9}$$

where $d_* = \sqrt[3]{(s-1) g / v^2}\, d_{50}$ is the dimensionless grain size.

The sediment diffusivity was related to the energy dissipation from wave breaking according to Karambas and Koutitas (2002).

The nearshore morphological changes are calculated by solving the conservation of sediment transport equation:

$$\frac{\partial z_b}{\partial t} = -\frac{\partial}{\partial x}\left(q_x - 5|q_x|\frac{\partial z_b}{\partial x}\right) - \frac{\partial}{\partial y}\left(q_y - 5|q_y|\frac{\partial z_b}{\partial y}\right) \tag{10}$$

where z_b is the local bottom elevation and q_x, q_y are the total volumetric longshore and cross-shore sediment transport rates (sum of bed and suspended load, derived from eqs 5 and 8).

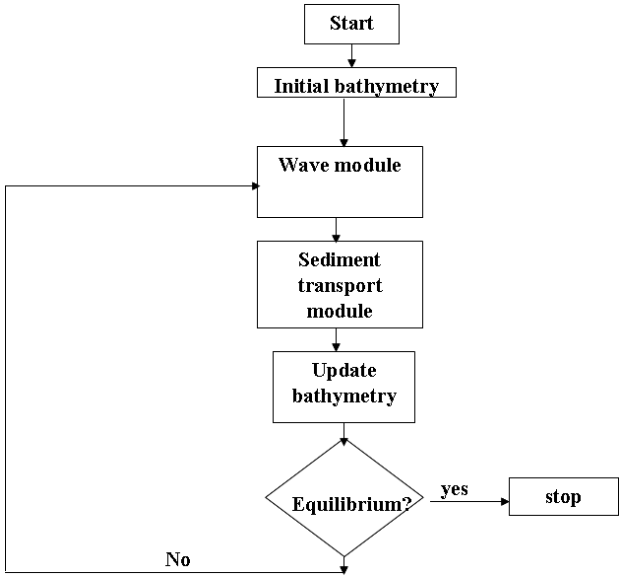

Figure 1. Structure of the morphological modelling system.

MORPHOLOGICAL CHANGES BEHIND DETACHED BREAKWATERS AND MODEL VERIFICATION

In order to study the effect of the detached breakwaters on the morphology of the coastal area and to verify also the model, a series of applications have been conducted. The following methodology has been adopted: first, the initial bathymetry was inserted into the model so as to estimate the wave and current field, which are used by the sediment transport model for the calculations of the sediment transport rates. Then, the bathymetry was updated according to the sediment movement, by solving the conservation of sediment transport equation. This procedure was repeated until the state of equilibrium was reached or after a specific period. The diagram in Fig. 1 shows the sequence in which the modules of the present model are run.

Reproduction of Ming and Chiew (2000) experiments

The present model is mainly verified against the laboratory experiments, by Ming and Chiew (2000) which depict the bathymetry changes behind a detached breakwater. The experiments were conducted in a wave basin that was 10 m long, 5 m wide, and 0.7 m high. A plunger-type wavemaker was used to generate monochromatic waves. Sponge was placed behind the wavemaker to minimize wave reflection. The 6 m long beach consisted of uniformly distributed sand with a median grain size of d_{50} = 0.25 mm. The test duration was approximately 15 h, which also was the duration needed for the beach to reach equilibrium. At the equilibrium stage, the waves tend to break simultaneously and normal to the shoreline and wave runup and rundown are almost perpendicular to the shoreline. Consequently, since the wave induced current is relatively weak, the sediment transport is insignificant and there is no noticeable advancement or recession of the shoreline for a duration of 2 hours.

Four different cases are reproduced numerically. The test conditions, as well as the information of formation of salient or tombolo, are presented in Table 1. The period of the incident wave was T=0.85 s and the height H_o=0.05 m.

Table 1. Experimental test conditions (Ming and Chiew, 2000)

Test	*B* (Breakwater length in m)	*X* (Distance from the initial shoreline in m	*B/X*	Formation of salient/tombolo
3	1.5	0.6	2.5	Tombolo
9	0.9	1.2	0.75	Salient
8	0.6	1.2	0.5	Salient
11	1.5	1.2	1.25	Tombolo

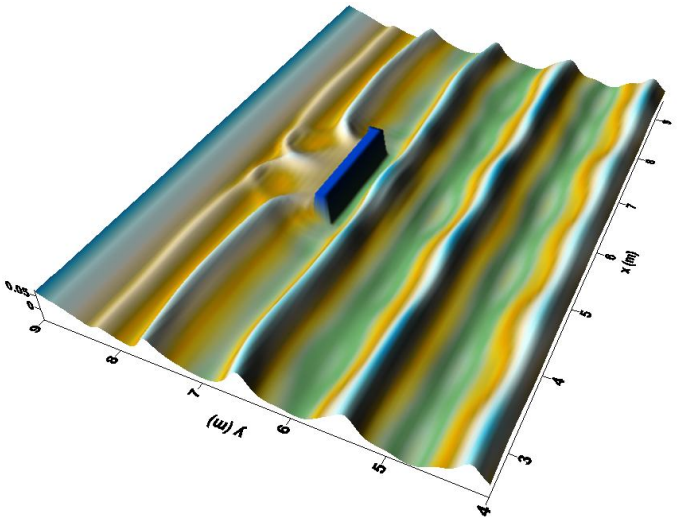

Figure 2. Snapshot of the computed free surface elevation of Test 11 (initial bathymetry).

In Fig. 2 a snapshot of the computed free surface elevation of Test 11, is shown. Wave shoaling, breaking, diffraction into the sheltered area as well as run-up and run-down, are shown in the figure.

Fig. 3 shows the wave induced current velocity filed and the initial bathymetry of Test 11.

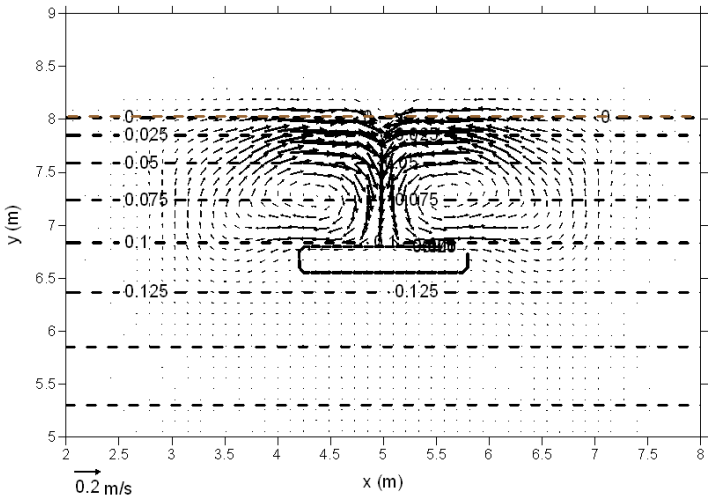

Figure 3. Initial bathymetry (dashed lines) and velocity field of Test 11.

Two circulation currents were formed behind the breakwater. The currents move towards the sheltered area along the foreshore from both sides of the breakwater so that two eddies develop. A secondary cause of the circulation currents is the gradient of the mean sea level between the illuminated area and the sheltered area due to diffraction effects (Fig. 2). It is obvious also that the wave motion in the swash zone, which is simulated by the model, contributed directly to the formation of the circulation currents.

In Fig. 4 the wave induced current velocity filed and the bathymetry after 1 hour of wave action is shown. The currents carried the eroded sediment to the sheltered area behind the breakwater. The sediment transport in the lee of the breakwater decreases due to the attenuated wave in the area sheltered by the breakwater. This causes the trapping of sand behind the breakwater and the formation of a salient.

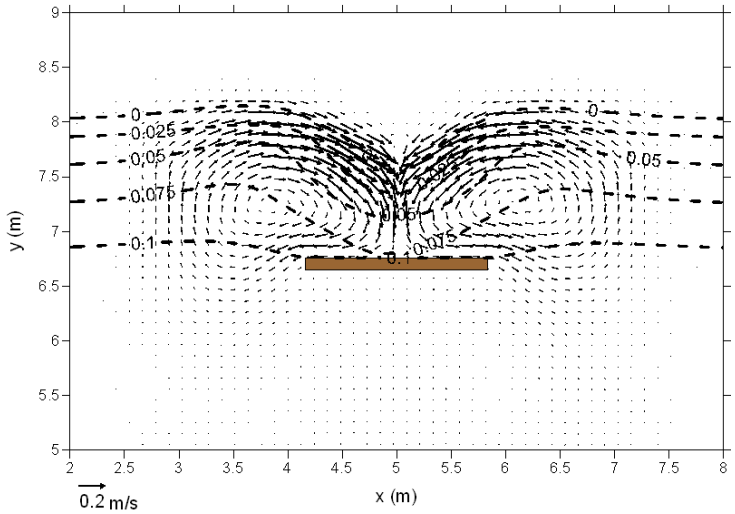

Figure 4. Bathymetry (dashed lines) and velocity field of Test 11, after 1 hour of wave action.

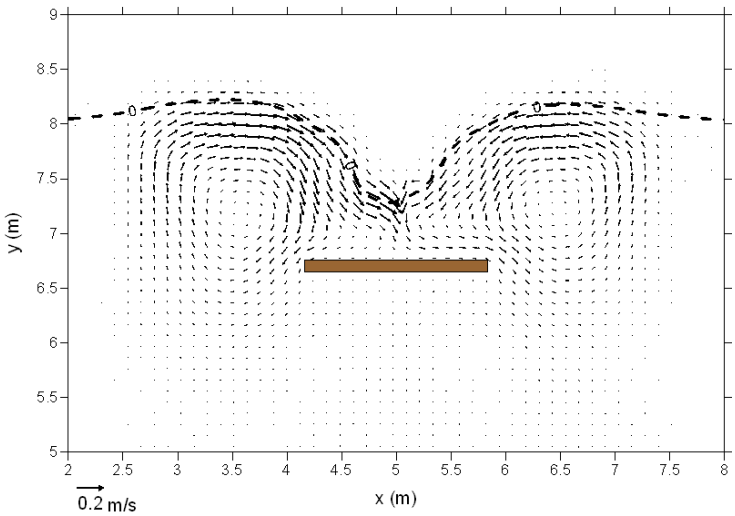

Figure 5. Bathymetry (dashed lines) and velocity field of Test 11, after 2 hours of wave action.

Fig. 5 shows the velocity field and the updated bathymetry after 2 hours of wave action. The currents are weaker than those of Figs 3 and 4. Fig. 6 shows the velocity field and the final bathymetry after 8 hours of wave action, where the equilibrium stage is reached.

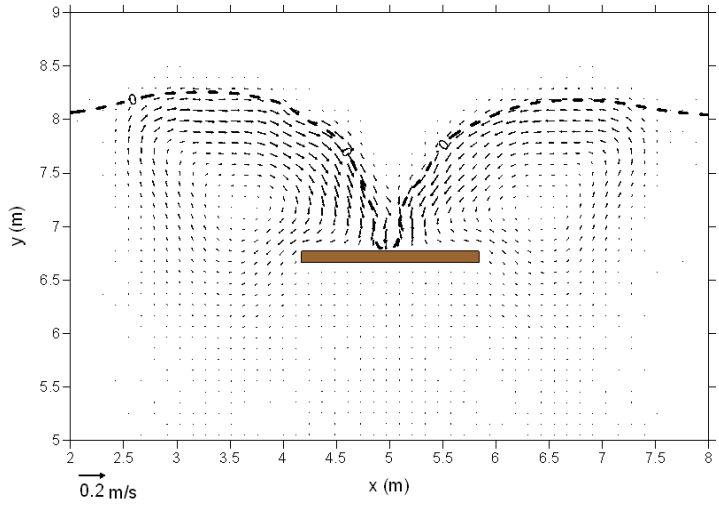

Figure 6. Final bathymetry (dashed lines) and velocity field of Test 11, after 8 hours of wave action.

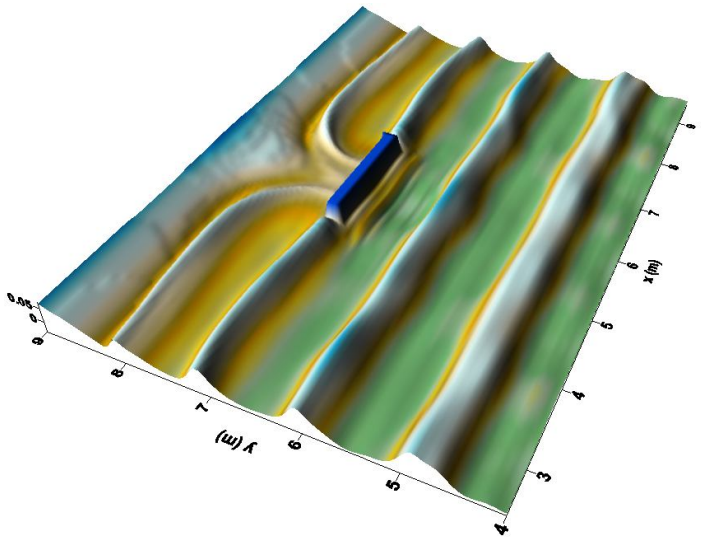

Figure 7. Snapshot of the computed free surface elevation of Test 11 (final bathymetry).

By comparing Figs 4, 5 and 6 it is concluded that the rate of the salient growth was high initially, and it slowed down as equilibrium was approached. In Fig. 7 a snapshot of the computed free surface elevation at the equilibrium stage is shown. At the equilibrium stage, the waves tend to break simultaneously and normal to the shoreline and wave runup and rundown are almost perpendicular to the shoreline. Consequently, since the wave induced current is relatively weak (Fig. 6), the sediment transport is insignificant and there is no noticeable advancement or recession of the shoreline.

Behind the structure, after equilibrium was reached, the shoreline extends out, thus forming a tombolo. Fig. 8 shows a comparison between the model results and the experimental data. The model can predict fairly well the coastal changes.

Notice that the *B/X* ratio is equal to 1.25, which agrees with the tombolo criterion found in the literature (Rosati, 1990, http://www.coastalwiki.org/coastalwiki/Detached_breakwaters).

In Fig 9 model results are compared with experimental data of Test 3. Again the model is able to simulate fairly well the morphological changes. The formation of tombolo is expected due to the large value of the ratio *B/X* (*B/X*=2.5).

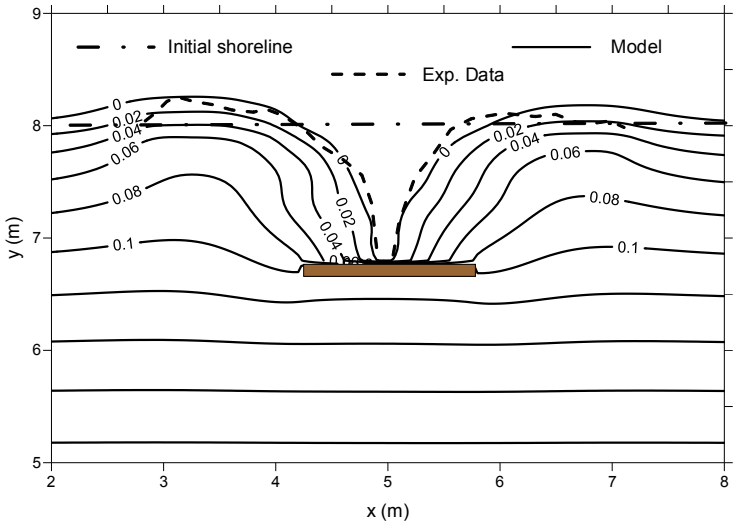

Figure 8. Comparison of model results and experimental data: Test 11 (final bathymetry).

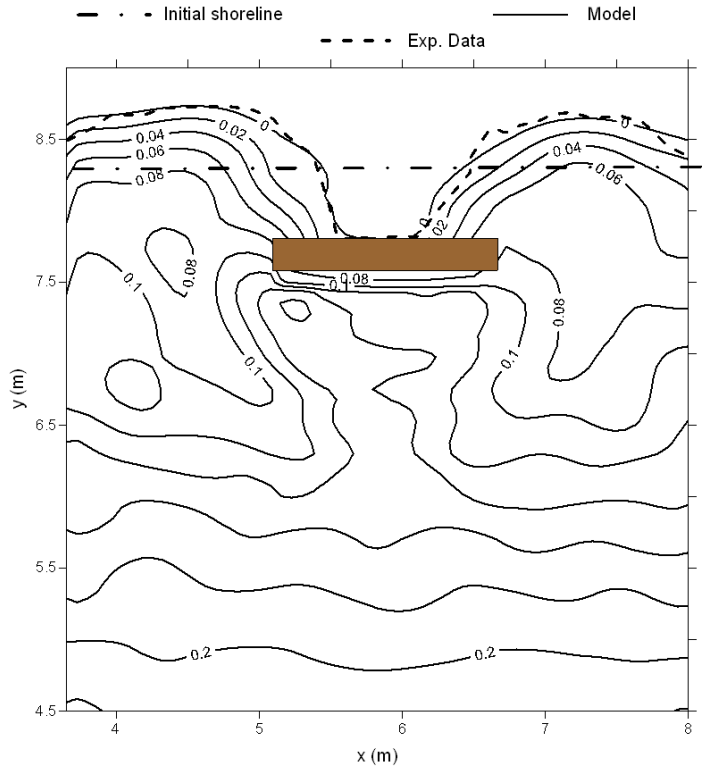

Figure 9. Morphology evolution behind a detached breakwater. Comparison of model results and experimental data: Test 3 (*B/X*=2.5).

In Fig 10, model results are compared with experimental data of Test 8. In the same figure the velocity field is also shown. As expected, due to the small value of the *B/X*, the sheltered area behind the detached breakwater, is smaller than in Test 11, and consequently the velocity field area is also smaller. Salient formation is predicted, since the ratio *B/X* is less relatively small (*B/X* =0.5). Model and laboratory results are in close agreement.

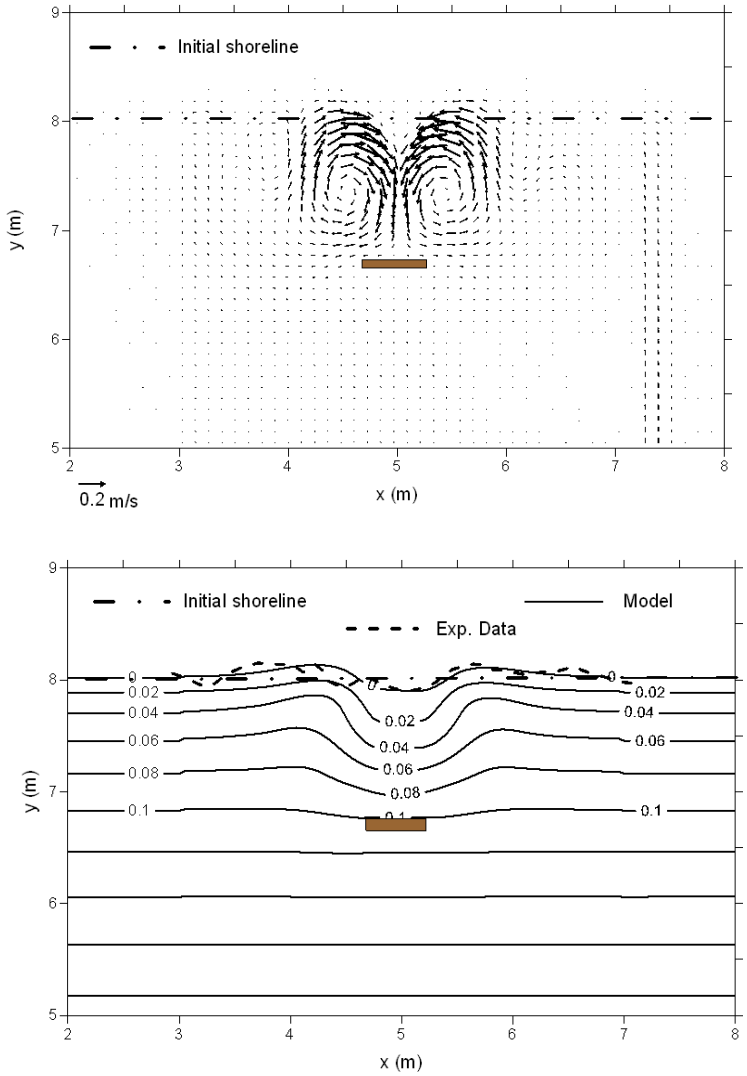

Figure 10. Velocity field and morphology evolution behind a detached breakwater. Comparison of model results and experimental data: Test 8 (*B/X* =0.5).

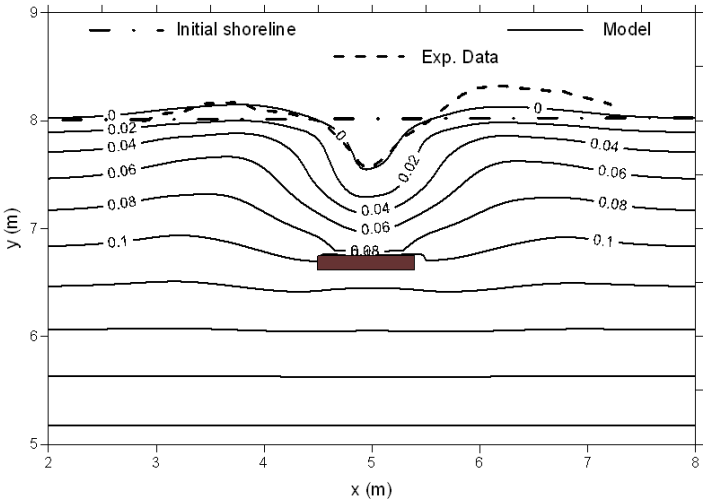

Figure 11. Morphology evolution behind a detached breakwater. Comparison of model results and experimental data: Test 9 (*B/X*=0.75).

In Fig 11, model results are compared with experimental data of Test 9. Again model results and laboratory data agree quite well. In this case also, salient formation is predicted, since the ratio *B/X* is less unity (*B/X* =0.75).

Similar good results are obtained by reproducing also the other Ming and Chiew (2000) tests.

In a similarity to the Ming and Chiew (2000) tests an additional test is conducted: breakwater length: *B*=0.40 m, distance from the shoreline: *X*=1.20 m, *B/X*=0.33. Wave height and period remained the same. Figure 12 shows the calculated bed levels after 8 hours (equilibrium stage). It can be seen that the detached breakwater has a minimal impact to the coastal morphology, due to the small value of the ration *B/X*.

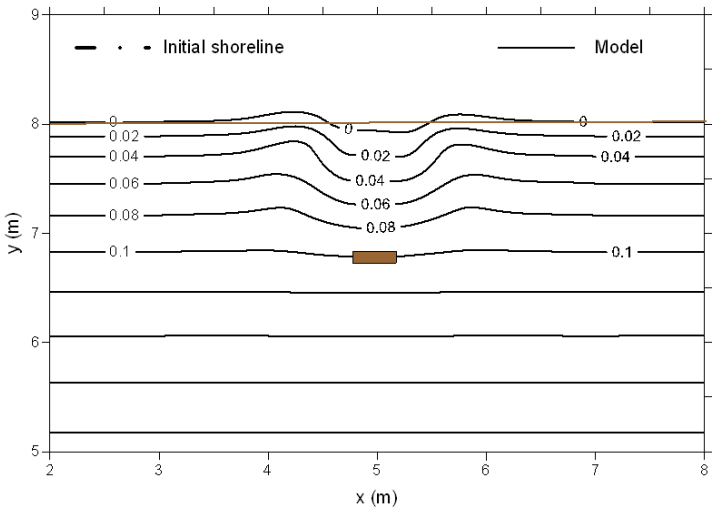

Figure 12. Morphology evolution behind a detached breakwater; *B*=0.40 m, *X*=1.20 m, *B/X* =0.5.

Based on model results the following design consideration can be derived:

B/X>1.2-1.3 Tombolo formation

0.2-0.3 <*B/X*<1.2-1.3 Salient formation

B/X<0.2-0.3 Minimal impact

which are in a general agreement with the design consideration found in the literature (Rosati, 1990).

Reproduction of Gravens and Wang (2007) experiments

A series of movable bed physical model experiments were carried out in the LSTF at the Coastal and Hydraulics Laboratory of the U.S. Army Engineer Research and Development Center in Vicksburg, Mississippi by Gravens and Wang (2007). Four series of experiments were designed to generate data sets for testing and validation of the development of tombolos in the lee of nearshore detached breakwaters and T-head groins. Spilling breaking waves were generated by four wave generators. The beach consisted of very well-sorted fine quartz sand with a median grain size of 0.15 mm. The longshore current generated by the obliquely incident waves was circulated with twenty turbine pumps through twenty flow channels at the updrift and downdrift ends of the basin. In this study, the T1C4 Test (detached breakwater) is used for validation of the model. The offshore wave condition were: zero moment wave height of spectral waves (TMA spectrum) H_{om}=0.225 m, peak period T_p=1.46 s and incident angle θ=6.5^o. In T1C4, a 4-m long detached breakwater was constructed parallel to the initial shoreline (*B*=4 m). The distance from the breakwater to the shoreline was 4 m (*X*=4 m).

Figure 13 shows the spatial distribution of calculated significant wave height and wave induced current field for Test T1C4. The calculation shows one eddy was created on the right of the detached breakwater (instead of two symmetric eddies if the incident wave direction is perpendicular to the shoreline).

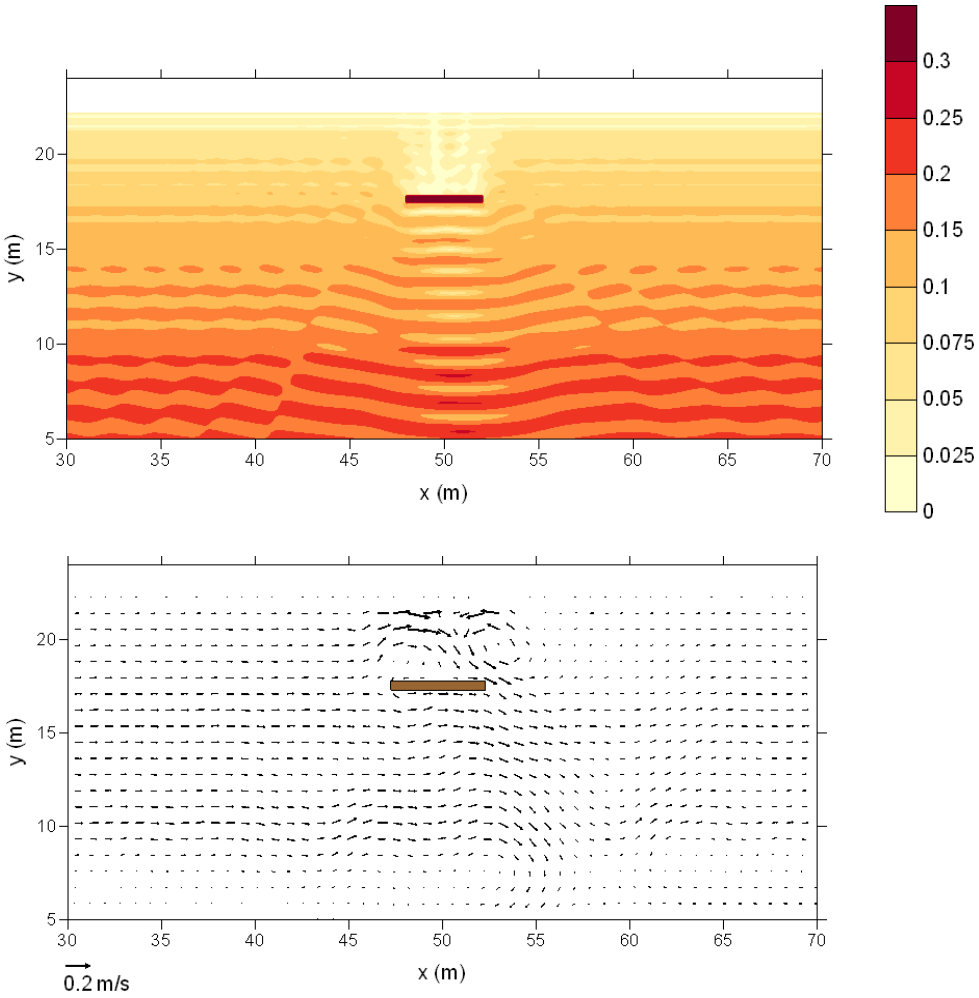

Figure 13. Spatial distribution of calculated significant wave height and wave induced current field; Gravens and Wang (2007) experiments, Test T1C4.

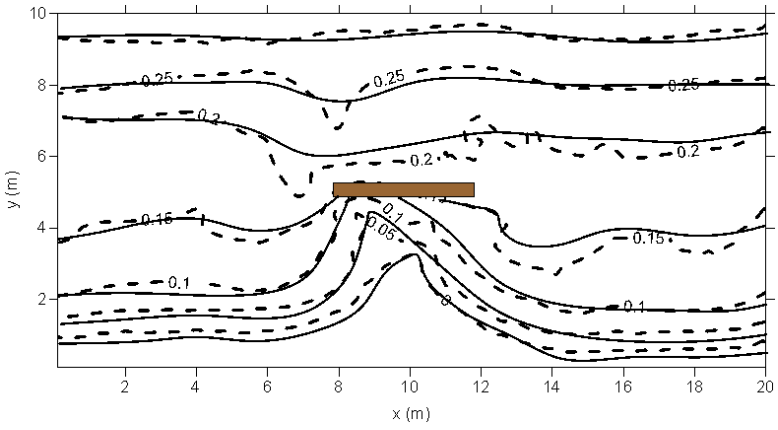

Figure 14. Comparison between the calculated and measured bed levels after 190 min for T1C4.

Figure 14 shows a comparison between the calculated and measured bed levels after 190 min for T1C4. The simulated beach morphological evolution in the vicinity of the detached breakwater agreed well with the experimental data.

APPLICATION TO CROSS-SHORE COASTAL EROSION

In this paragraph the model is applied to estimated innovative submerged structures effects on cross-shore sediment transport and beach morphology evolution.

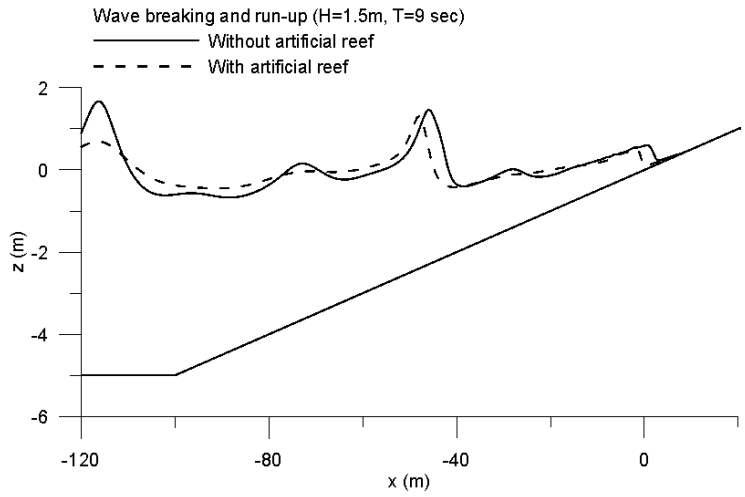

Figure 15. Breaking and runup of regular wave with or without submerged structures ('Reef Ball' type artificial reef).

In figure 15 breaking and run-up of regular waves on a 1/20 slope, with and without the presence of a artificial reef, is shown (Wave height H=1.5 m, period T=11 sec). The transmission coefficient is about 0.6 ($K_t \approx 0.6$). The transmission coefficient is defined as the ratio of the transmitted wave height to the incident wave height. With the presence of artificial reef ('Reef Ball' type, Harris, 2009), the incident wave height is reduced, and consequently breaking occurs closer to the shore line resulting to milder hydrodynamics conditions within the surf and swash zone. The presence of the 'Reef Ball' type artificial reef is incorporated according to Karambas et a. (2012).

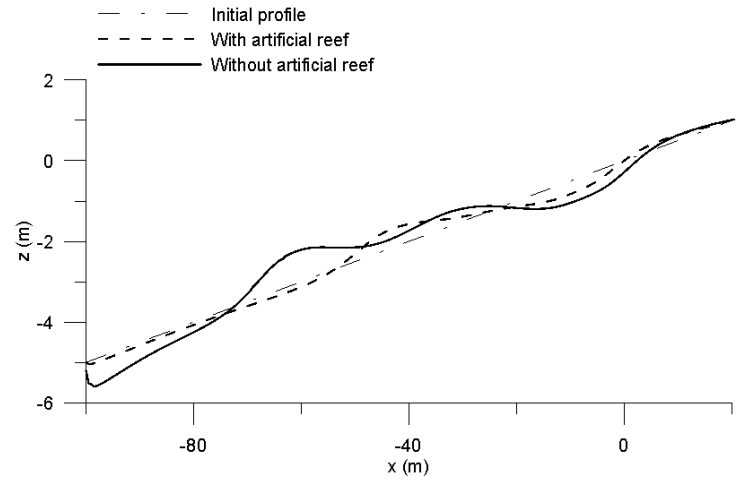

Figure 16. Cross-shore morphology evolution with and without artificial reef.

In Figure 16 cross-shore morphology evolution after 6 hr of wave action is shown. In the numerical experiment a grain size of d_{50}=0.3 mm is considered It is obvious that despite the relatively large value of the transmission coefficient, when artificial reef is present (K_t≈0.6), the reduction of the erosion is obvious. Notice that a transmission coefficient K_t≈0.6 corresponds to 36% wave energy transmission. This energy reduction seems to be quite significant.

CONCLUSIONS

An advanced nonlinear wave, sediment transport and bed morphology evolution 2DH model has been developed. Model results, i.e. morphology evolution behind detached breakwater, are compared with experimental data. The agreement between numerical simulations and data is quite satisfactory. The formation of tombolo or salient is automatically reproduced and agrees with the literature. The methodology can be applied to design coastal shore protection structures, such as detached breakwaters.

ACKNOWLEDGMENTS

The support of the European Commission through FP7.2009-1, Contract 244104 - THESEUS ("Innovative technologies for safer European coasts in a changing climate"), is acknowledged.

REFERENCES

Camenen, B., Larson, M. 2007. *A unified sediment transport formulation for coastal inlet application*, Technical report ERDC/CHL CR-07-1, US Army Engineer Research and Development Center, Vicksburg, MS.

Camenen, B., Larson, M. 2005. A general formula for non-cohesive bed load sediment transport, *Estuarine, Coastal and Shelf Science* 63, 249-260.

Camenen, B., Larson, M. 2008. A general formula for noncohesive suspended sediment transport, *Journal of Coastal Research* 24(3), 615-627.

Chen Q., Dalrymple, R.A., Kirby, J.T., Kennedy, A.B. and Haller M.C. 1999. Boussinesq modelling of a rip current system, *Journal of Geophysical Research*, 104(C9), pp. 20617-20637.

Harris L.E. 2009. Artificial Reefs for Ecosystem Restoration and Coastal Erosion Protection with Aquaculture and Recreational Amenities. *Reef Journal*, Vol. 1 No. 1, pp. 235-246.

Karambas Th. V. and C. Koutitas. 2002. Surf and swash zone morphology evolution induced by nonlinear waves, *Journal of Waterway, Port, Coastal and Ocean Engineering*, American Society of Civil Engineers (ASCE), Vol. 128, no 3, pp. 102-113.

Karambas Th. V. 2002. Nonlinear Wave Modeling and Sediment Transport in the Surf and Swash Zone, *ADVANCES in COASTAL MODELING*, Elsevier Science Publishers.

Karambas Th. V. and E.K. Karathanassi. 2004. Boussinesq modeling of Longshore currents and sediment transport, *Journal of Waterway, Port, Coastal and Ocean Engineering*, American Society of Civil Engineers (ASCE), Vol. 130, no 6, pp. 277-286.

Karambas Th. V. 2006. Prediction of sediment transport in the swash zone by using a nonlinear wave model, *Continental Shelf Research*, 26, pp. 599-609.

Karambas Th., Ch. Koftis, E. Koutandos and P. Prinos. 2012. Innovative Submerged Structures/Vegetation Effects on Coastal Erosion: Numerical Modeling of Hydro-Morphological Processes, *Proceedings of the Twenty-second International Offshore and Polar Engineering Conference*, Rhodes, Greece.

Kobayashi, N., Agarwal, A., and Johnson, B. 2007. Longshore Current and Sediment Transport on Beaches. *J. Waterw., Port, Coastal, Ocean Eng.*, 133(4), 296–304

Gravens, M.B., Wang, P. 2007. *Data report: laboratory testing of longshore sand transport by waves and currents; morphology change behind headland structures*. Technical Report, ERDC/CHL TR-07-8, Coastal and Hydraulics Laboratory, US Army Engineer Research and Development Center, Vicksburg, MS.

Lynett P. J., J. A. Melby, D-H Kim. 2010. An application of Boussinesq modeling to Hurricane wave overtopping and inundation. *Ocean Engineering*, 37, pp. 135–153.

Militello A., C. W. Reed, A.K. Zundel, N. C. Kraus. 2004. *Two-Dimensional Depth-Averaged circulation model M2D: version 2.0, Report 1*, US Army Corps of Engineers, ERDC/CHL TR-04-2.

Ming D. and Y-M. Chiew. 2000. Shoreline changes behind detached breakwater, *Journal of Waterway, Port, Coastal, and Ocean Engineering*, Vol. 126, No. 2, 63-70.

Ribberink J.S. 1998. Bed-load transport for steady flows and unsteady oscillatory flows, *Coastal Engineering*, 34, pp.59-82.

Rosati J.D. 1990. *Functional design of breakwaters for shore protection: empirical methods Technical Report*, CERC-90-15, US Army Corps of Engineers, Washington DC.

Schäffer H. A., Madsen P.A. and Deigaard R. 1993. A Boussinesq model for waves breaking in shallow water, *Coastal Engineering*, 20, pp. 185-202.

Sørensen O.R., Schäffer H. A., Madsen P.A. 1998. Surf zone dynamics simulated by a Boussinesq type model. Part III. Wave-induced horizontal nearshore circulations. *Coastal Engineering*, 33, pp 155-176.

Wei G. and Kirby T. 1995. Time-dependent numerical code for extended Boussinesq equations. *Journal of Waterway, Port, Coastal, and Ocean Engineering*, vol. 121, no 5, pp. 251-261

Wenneker I., Ap van Dongeren, J. Lescinski, D. Roelvink, M. Borsboom. 2011. A Boussinesq-type wave driver for a morphodynamical model to predict short-term morphology, *Coastal Engineering*, 58, pp. 66–84.

Zou Z.L. 1999. Higher order Boussinesq equations, *Ocean Engineering*, 26, pp. 767-792.